Composites Science and Technology 223 (2022) 109408

Contents lists available at ScienceDirect

Composites Science and Technology

journal homepage: www.elsevier.com/locate/compscitech

Electromechanical characterization and kinetic energy harvesting of piezoelectric nanocomposites reinforced with glass fibers

Kohei Maruyama [a], Yoshihiro Kawakami [b], Kotaro Mori [c], Hiroki Kurita [a], Yu Shi [d], Yu Jia [e], Fumio Narita [a,*]

[a] Department of Frontier Sciences for Advanced Environment, Graduate School of Environmental Studies, Tohoku University, Sendai, 980-8579, Japan
[b] Research Institute for Electromagnetic Materials, Tomiya, 981-3341, Japan
[c] Department of Mechanical System Engineering, College of Engineering, Ibaraki University, Hitachi, 316-8511, Japan
[d] Department of Mechanical Engineering, University of Chester, Chester, CH2 4NU, UK
[e] Department of Mechanical Engineering, Aston University, Birmingham, B4 7ET, UK

A B S T R A C T

Piezoelectric composites are a significant research field because of their excellent mechanical flexibility and sufficient stress-induced voltage. Furthermore, due to the widespread use of the Internet of Things (IoT) in recent years, small-sized piezoelectric composites have attracted a lot of attention. Also, there is an urgent need to develop evaluation methods for these composites. This paper evaluates the piezoelectric and mechanical properties of potassium sodium niobate (KNN)-epoxy and KNN-glass fiber-reinforced polymer (GFRP) composites using a modified small punch (MSP) and nanoindentation tests in addition to d_{33} measurements. An analytical solution for the piezoelectric composite thin plate under bending was obtained for the determination of the bending properties. Due to the glass fiber inclusion, the bending strength increased by about four times, and Young's modulus in the length direction increased by approximately two times (more than that of the KNN-epoxy); however, in the thickness direction, Young's modulus decreased by less than half. An impact energy harvesting test was then performed on the KNN-epoxy and KNN-GFRP composites. As a result, the output voltage of KNN-GFRP was larger than that of KNN-epoxy. Also, the output voltage was about 2.4 V with a compressive stress of 0.2 MPa, although the presence of the glass fibers decreased the piezoelectric constants. Finally, damped flexural vibration energy harvesting test was carried out on the KNN-epoxy and KNN-GFRP composites. The KNN-epoxy was broken during the test, however KNN-GFRP composite with a load resistance of 10 MΩ generated 35 nJ of energy. Overall, through this work, we succeeded in developing piezoelectric energy harvesting composite materials that can withstand impact and bending vibration using glass fibers and also established a method for evaluating the electromechanical properties with small test specimen.

1. Introduction

Piezoelectric materials can convert mechanical and electrical energy with high efficiency and are mainly applied to sensors and actuators. Furthermore, piezoelectric materials are also expected to be utilized as virus sensors [1–3]. In recent years, many research types have been conducted on energy harvesting materials [4–10].

The most commonly used piezoelectric material, lead zirconate titanate (PZT), has extensive piezoelectric properties. However, the Restriction of Hazardous Substances, which came into effect in Europe in 2006, regulates the use of lead. Also, piezoelectric materials, especially ceramics, are incredibly brittle and have the disadvantage of cracking [11–15] during manufacturing and service. To solve this problem, methods such as protecting piezoelectric materials with other protective materials are considered, but they are challenged with other problems, such as the device size and the cost of the protective materials.

There are piezoelectric composite materials in which piezoelectric and polymer materials are combined to overcome drawbacks such as the brittleness of piezoelectric materials [16–20]. Piezoelectric composites with high toughness are essential in energy harvesting, and this topic has been attracting a lot of attention [21–27]. However, devices that convert vibration and shock energy into electrical energy have the problem of how they will be damaged after long-term use, resulting in drastic decreases in power generation. Therefore, it is necessary to secure sufficient strength to prevent piezoelectric materials from being damaged in the devices used for extended time.

Piezoelectric energy harvesting composite materials can result in catastrophic failures under vibration, and they need to be reinforced so that their durability can be improved. Glass fiber-reinforced polymers (GFRPs) [28] and carbon fiber-reinforced polymers (CFRPs) [29] with piezoelectric performances have been developed. For example, Wang et al. [30] fabricated potassium sodium niobate (KNN) piezo resin composites and polarized the composites successfully using CFRP electrodes. Then, they evaluated the output power characteristics under

* Corresponding author.
E-mail address: narita@material.tohoku.ac.jp (F. Narita).

https://doi.org/10.1016/j.compscitech.2022.109408
Received 22 October 2021; Received in revised form 16 March 2022; Accepted 18 March 2022
Available online 21 March 2022

impact and vibration tests. Also, Takaishi et al. [31] fabricated mullite ceramic fiber/thermoplastic polymer piezoelectric composites and evaluated their performance. To design and develop high-performance and long-life vibration energy harvesting composite materials, evaluations of the strength, fracture properties, output voltage, and power limits are vital. Hence, it is necessary to use small test specimens. Thus, a new evaluation method for determining the strength and fracture properties of energy harvesting piezoelectric composite materials using small test specimens is needed.

In this work, we aimed to fabricate GFRP composite materials using an epoxy resin mixed with lead-free piezoelectric nanoparticles. Then, we evaluated the electromechanical properties of the proposed GFRP composite materials. Modified small punch (MSP), nanoindentation, and compressive impact and damped flexural vibration tests were conducted on the piezoelectric GFRP composites to evaluate the Young's modulus, bending strength, MSP energy, and compressive and bending stress-induced output voltage. Also, analytical solutions for an axisymmetric piezoelectric material were derived under a uniformly distributed load inside a concentric circle while considering the associated electromechanical interactions. The performance of the piezoelectric GFRP composite was compared with that of a piezoelectric resin without glass fibers.

2. Experimental procedure

2.1. Material preparation

Two types of piezoelectric composites were considered, one with glass fibers and the other without glass fibers. Fig. 1 (a) and (b) show schematic diagrams of the piezoelectric composites without and with glass fibers, respectively. The piezoelectric composite was made using a piezoelectric resin with a length of 20 mm, a width of 12 mm, and a thickness of 0.4 mm; glass fibers, and conductive tape (copper foil). The tape's length, width, and thickness are 18 mm, 10 mm, and 0.2 mm, respectively. Two-component epoxy resin (Bisphenol F resin; Sumita Science and Technology Laboratory Co., Ltd.) and ST12 (epoxy resin curing agent; Mitsubishi Chemical) were used as base materials to prepare the piezoelectric resin. Also, sodium niobate $K_{1-x}Na_xNbO_3$ (KNN) particles (Nippon Chemical Industrial Co., Ltd.) were used. The KNN particles and epoxy resin were mixed at a mass ratio of 64:36 to a volume content of 32 %. After stirring with a spoon for 10 min, the mixture was further stirred for 5 min using a stirrer (AR-100, THINKY Corp.). Then, it was defoamed for 5 min. In the sample piece without glass fibers, the stirred piezoelectric resin was uniformly applied onto the aluminum plate. To adjust the thickness of the sample, a 0.40-mm thick Teflon sheet was sandwiched, and an aluminum plate of the same size was placed on top of it. Then, they were fixed with screws and compressed. Afterward, the resulting sheet was cured in a thermostat (DVS402, Yamato Scientific Co., Ltd.) at 135 °C for 1 h. After curing, the produced piezoelectric resin sheet was cut and polished, and a conductive tape was attached to it as an electrode. In the case of the sample with glass fiber, the stirred piezoelectric resin was uniformly applied to an aluminum plate. Then, two layers of glass cloth were placed, and the piezoelectric resin was infiltrated into the glass cloth. Afterward, the sheet was cured using the same way as mentioned above. Fig. 1(c) shows the scanning electron microscope (SEM) (SU-70, Hitachi

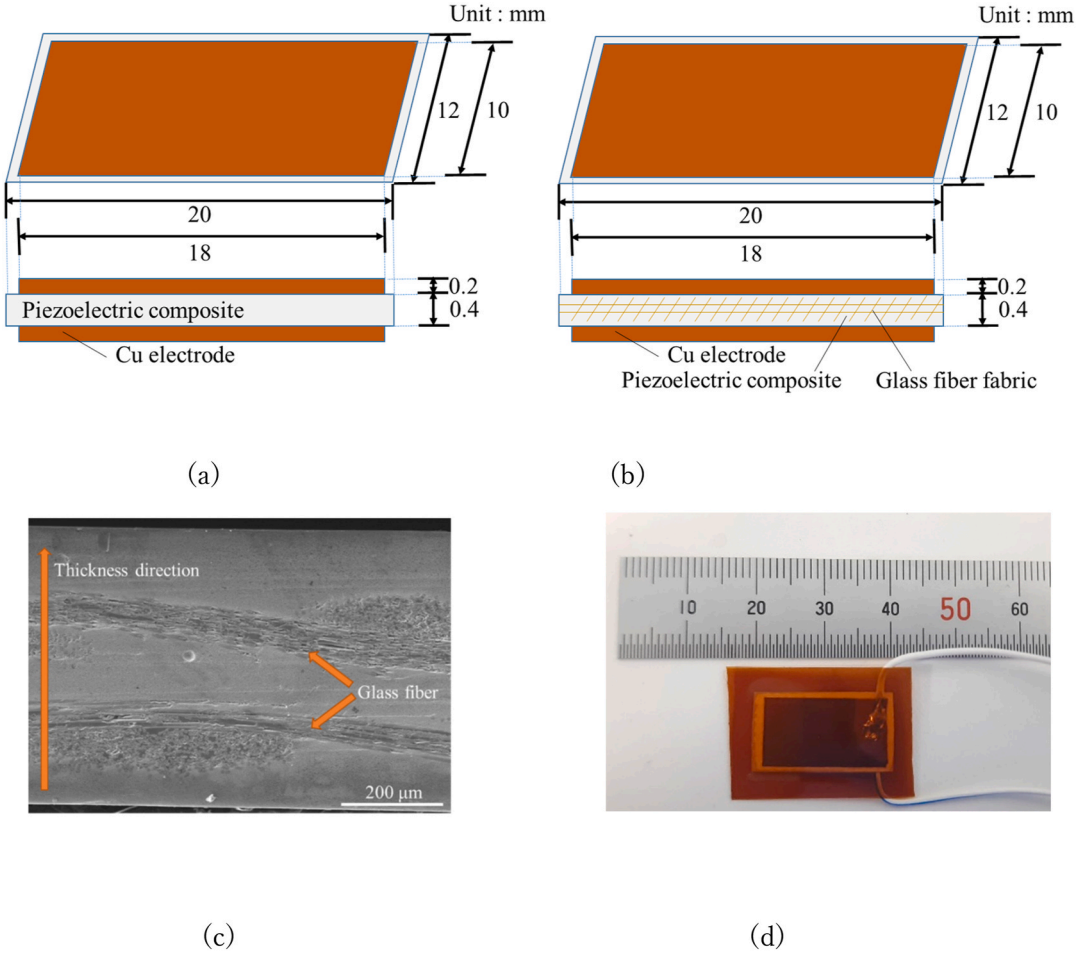

Fig. 1. Schematic diagram of the piezoelectric composite samples (a) without and (b) with glass fibers; (c) SEM image of the KNN-GFRP sample; (d) photograph of the specimen.

Co., Ltd.) image of the cross-section of the KNN-GFRP sample, and Fig. 1 (d) shows the prepared sample. The volume content of KNN was approximately 20 %.

2.2. Modified small punch test

A test sample with dimensions of 10 mm × 10 mm × 0.4 mm was cut out. The surface of the sample was polished to # 1200 on both sides using abrasive paper. The MSP test was performed using a 5-kN universal tester (AG-5kNXD, Shimadzu Corp.), and the load was applied on the test sample with a crosshead speed of 0.1 mm/min. The load was applied with cylindrical stainless steel. Fig. 2(a) shows a photograph of the MSP test jig, and Fig. 2(b) shows a schematic diagram of the MSP test. Here, the radius of the lower die hole is 2.1 mm, and the radius of the puncher is 1.175 mm.

2.3. Nanoindentation test

The elastic properties of the piezoelectric composites were evaluated in accordance with ISO14577 [32]. A TTX-NHT^3 (Anton Paar Inc.) with a Berkovich indenter tip was used, and the maximum load was 500 mN. More than ten indentations were made in each test sample, and an average of these indentations was obtained. Young's modulus (Y_{33}) in the thickness direction was determined using the Oliver & Pharr analysis.

2.4. Poling treatment

The piezoelectric composites were polarized using the corona discharge polarization method, and a corona discharge device (ELC-01N, Element Co., Ltd.) was used. The polarization treatment conditions were performed for all the samples at a hot plate temperature of 100 °C, an applied voltage of 8 kV, and an applied time of 10 min.

2.5. Piezoelectric constant measurement

Each polarized sample was placed between the upper and lower probes of the force head. The center of the sample was fixed, and the piezoelectric constant was measured using a d_{33} meter (YE2730A, Sinoceramics, Inc.).

2.6. Impact output voltage measurement

Fig. 3 shows a schematic diagram of the impact energy harvesting test. First, the test sample (KNN-epoxy and KNN-GFRP) was connected to an oscilloscope (MDO3024, Tektronix, Inc.) and fixed on the central axis of the head of the impact load device. After that, compressive loads of 0.10, 0.15, and 0.20 MPa were applied ten times under the conditions of a load time of 0.1 s and a load interval of 3.0 s, and the generated voltage by the impact was measured.

2.7. Damped flexural vibration output voltage measurement

A test sample (KNN-epoxy and KNN-GFRP) with dimensions of 10 × 45 × 0.6 mm^3 was cut out, and gold electrodes were deposited on the top side using a sputtering machine (SC-701MkII, Sanyu Electron Co., Ltd.). Then, the sample was polarized and attached to the stainless-steel plate (YUS205M1, NIPPON STEEL Chemical & Material Co., Ltd.) of 0.1 mm thickness by the conductive epoxy resin (CW2401, Chemtronics). After that, the sample was fixed to Acrylic resin block as shown in Fig. 4. Free length is 40 mm. Load resistance R_L was then connected in parallel to the samples, and damped vibration was applied by snapping the tip by 2 mm. An oscilloscope (TBS 1052B, Tektronix, Inc.) measured the output voltage with time. The accumulated energy due to the damped vibration was evaluated as the harvested energy [33].

3. Theoretical analysis of bending

3.1. Analytical procedure for the thin plate under open circuit condition

Let us now consider the rectangular Cartesian coordinates x_i(O-x_1,x_2,x_3). The constitutive relations [34] for the piezoelectric composite materials poled in the x_3- direction can be found in Appendix A. For a thin plate in the x_1x_2 plane, all the strain and stress components that are related to the x_3 coordinate can be neglected. The constitutive relations for the piezoelectric thin plate under the open circuit condition are also given in Appendix A.

Consider a piezoelectric composite plate with a thickness of h as shown in Fig. 5(a). Let the coordinate axes $x = x_1$ and $y = x_2$ be such that they are in the middle plane of the plate with the thickness of h, where the $z = x_3$ axis is normal to this plane. Also, suppose that the coordinate $z = 0$ is located on the neutral surface of the plate. Beckers

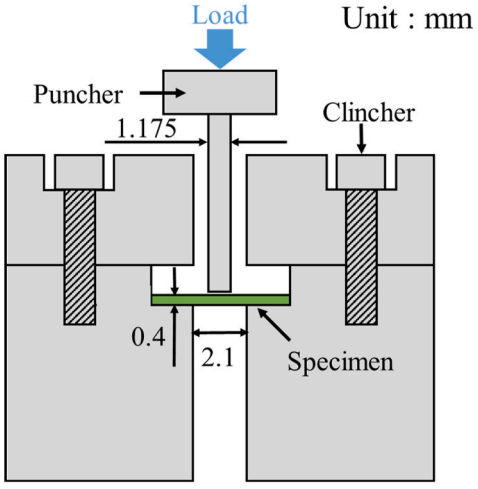

(a) (b)

Fig. 2. Schematic of the MSP test: (a) photograph and (b) schematic diagram.

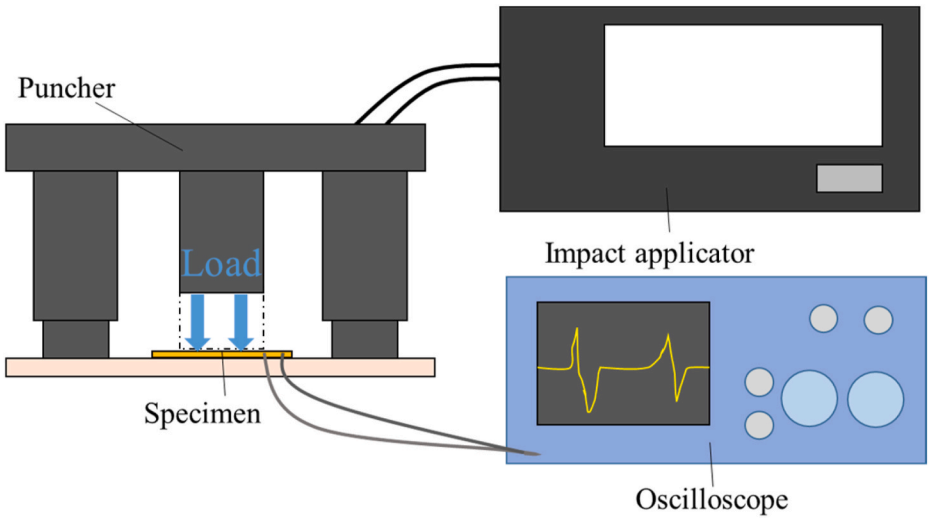

Fig. 3. Schematic diagram of the impact energy harvesting test.

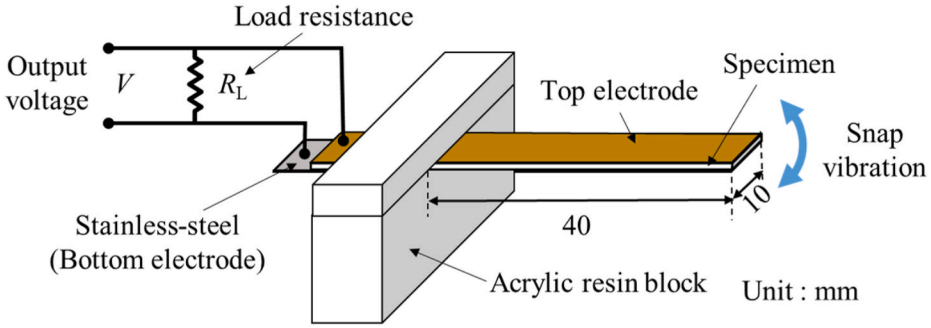

Fig. 4. Schematic diagram of the damped flexural vibration energy harvesting test.

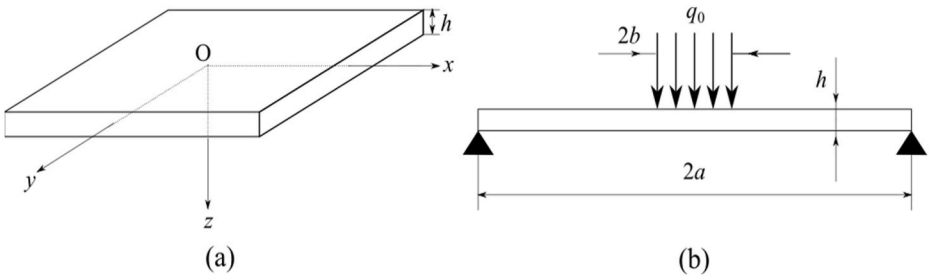

Fig. 5. Schematic drawing of (a) a thin plate and (b) a simply supported circular plate under a partially uniform distributed load.

and Dehez [35] developed the constitutive equations of piezoelectric laminated structures under bending load. They considered the translation of the arbitrary point on the neutral surface in the x- and y-directions as well as the out-of-plane displacement. For simplicity here, we ignore the neutral surface displacements in the x- and y-directions. According to the classical thin plate theory, the displacement components may be expressed as follows [36]:

$$u_x = -z\frac{\partial w}{\partial x},\ u_y = -z\frac{\partial w}{\partial y},\ u_z = w(x,y) \tag{1}$$

where $w(x,y)$ represents the deflection of the middle plane. The strains are defined in terms of displacement as follows:

$$\varepsilon_{xx} = \frac{\partial u_x}{\partial x},\ \varepsilon_{yy} = \frac{\partial u_y}{\partial y},\ \varepsilon_{xy} = \frac{1}{2}\left(\frac{\partial u_x}{\partial y} + \frac{\partial u_y}{\partial x}\right) \tag{2}$$

Thus, the strain variations within the plate are related to the deflection $w(x,y)$ by the following expressions:

$$\varepsilon_{xx} = -z\frac{\partial^2 w}{\partial x^2},\ \varepsilon_{yy} = -z\frac{\partial^2 w}{\partial y^2},\ \varepsilon_{xy} = -z\frac{\partial^2 w}{\partial x \partial y} \tag{3}$$

The stress equilibrium equations and stress boundary conditions on the plate surfaces are given in Appendix B.

From Eq. (B7), with the third of Eq. (A5), Eqs. (A8), (B3) and (3), we obtain

$$D\nabla^4 w = q \tag{4}$$

where the flexural stiffness D is obtained as follows:

$$D = \frac{h^3}{12}\frac{s_{11}^D}{\left(s_{11}^D\right)^2 - \left(s_{12}^D\right)^2} \tag{5}$$

By substituting Eq. (A9) into Eq. (5), then

$$D = \frac{h^3}{12}\frac{Y_{11}\left(1 - d_{31}^2/s_{11}\varepsilon_{33}\right)}{(1-\nu_{12}^2) - 2(1+\nu_{12})d_{31}^2/s_{11}\varepsilon_{33}} \tag{6}$$

If we consider the case where the piezoelectric plate is deformed under the short circuit condition, then Eq. (6) can be rewritten as follows:

$$D = \frac{h^3}{12}\frac{Y_{11}}{1-\nu_{12}^2} \tag{7}$$

This is equivalent to the flexural stiffness of the elastic composite materials that ignore the piezoelectric effect [37].

3.2. Solution for the circular axisymmetric plate under a uniformly distributed load inside a concentric circle

Let us now consider a circular piezoelectric composite plate with a radius a and a thickness h, as shown in Fig. 5(b). The origin of the coordinates (r, θ, z) coincides with the center of the circular plate. The plate is subjected to a uniformly distributed load q_0 in the area $0 \leqq r \leqq b$ of the upper surface. The moments can be reexpressed as follows:

$$M_{rr} = \int_{-h/2}^{h/2}\sigma_{rr}z\mathrm{d}z = -D\left(\frac{\nu^D}{r}\frac{\mathrm{d}w}{\mathrm{d}r} + \frac{\mathrm{d}^2 w}{\mathrm{d}r^2}\right) \tag{8}$$

$$M_{\theta\theta} = \int_{-h/2}^{h/2}\sigma_{\theta\theta}z\mathrm{d}z = -D\left(\frac{1}{r}\frac{\mathrm{d}w}{\mathrm{d}r} + \nu^D\frac{\mathrm{d}^2 w}{\mathrm{d}r^2}\right) \tag{9}$$

$$M_{r\theta} = 0 \tag{10}$$

where

$$\nu^D = -\frac{s_{12}^{\mathrm{D}}}{s_{11}^{\mathrm{D}}} \tag{11}$$

The equivalent shear force is given by

$$F = -D\left(-\frac{1}{r^2}\frac{\mathrm{d}w}{\mathrm{d}r} + \frac{1}{r}\frac{\mathrm{d}^2 w}{\mathrm{d}r^2} + \frac{\mathrm{d}^3 w}{\mathrm{d}r^3}\right) \tag{12}$$

Supposing that this plate bears a z-axis symmetric bending deflection under a uniform load q, we reexpressed Eq. (4) in the polar coordinate as follows:

$$\frac{1}{r}\frac{\mathrm{d}}{\mathrm{d}r}\left\{r\frac{\mathrm{d}}{\mathrm{d}r}\left[\frac{1}{r}\frac{\mathrm{d}}{\mathrm{d}r}\left(r\frac{\mathrm{d}w}{\mathrm{d}r}\right)\right]\right\} = \frac{q}{D} \tag{13}$$

For an axisymmetric bending deflection and under a uniformly distributed load q_0, as shown in Fig. 5(b), Eq. (13) has the following general solutions:

$$w_1(r) = \frac{1}{D}\left\{\frac{q_0}{64}r^4 + \left(C_1 r^2 + C_2\right)\log r + C_3 r^2 + C_4\right\}\ (0 < r < b) \tag{14}$$

$$w_2(r) = \frac{1}{D}\left\{\left(C_5 r^2 + C_6\right)\log r + C_7 r^2 + C_8\right\}\ (b < r < a) \tag{15}$$

where C_j ($j = 1, \ldots, 8$) are the integration constants. Note that the deflection $w_1(r)$ is a limited value at $r = 0$. Thus, the constant C_2 should be 0 in Eq. (14).

The boundary conditions are as follows:

$$\frac{\mathrm{d}w_1}{\mathrm{d}r} = 0\ (r = 0) \tag{16}$$

$$w_1 = w_2\ (r = b) \tag{17}$$

$$\frac{\mathrm{d}w_1}{\mathrm{d}r} = \frac{\mathrm{d}w_2}{\mathrm{d}r}\ (r = b) \tag{18}$$

$$\sigma_{rr1} = \sigma_{rr2}\ (r = b) \tag{19}$$

$$F_1 = F_2\ (r = b) \tag{20}$$

$$w_2 = 0\ (r = a) \tag{21}$$

$$\sigma_{rr2} = 0\ (r = a) \tag{22}$$

From these seven boundary conditions, we have

$$w_1(r) = \frac{q_0 b^2}{16D}\left[\frac{1}{4b^2}r^4 - \left\{\frac{4a^2 - (1-\nu^D)b^2}{2(1+\nu^D)a^2} + 2\log\left(\frac{a}{b}\right)\right\}r^2 + \frac{4(3+\nu^D)a^2}{4(1+\nu^D)} - \frac{(7+3\nu^D)}{4(1+\nu^D)}b^2 - b^2\log\left(\frac{a}{b}\right)\right] \tag{23}$$

$$w_2(r) = \frac{q_0 b^2}{16D}\left[\frac{3+\nu^D}{1+\nu^D}\left(a^2 - r^2\right) - 2r^2\log\left(\frac{a}{r}\right) - b^2\left\{\frac{(1-\nu^D)}{2(1+\nu^D)}\left(1 - \frac{r^2}{a^2}\right) + \log\left(\frac{a}{r}\right)\right\}\right] \tag{24}$$

By introducing the concentrated load $P = q_0\pi b^2$, the maximum deflection becomes

$$w_1(0) = \frac{P}{64\,\pi D}\left\{\frac{4(3+\nu^D)}{(1+\nu^D)}a^2 - \frac{(7+3\nu^D)}{(1+\nu^D)}b^2 - 4b^2\log\left(\frac{a}{b}\right)\right\} \tag{25}$$

Then, the maximum stress at $z = h/2$ becomes

$$\sigma_{rr1}(0) = \frac{3P}{2\pi h^2}\left\{1 - \frac{(1-\nu^D)}{4}\frac{b^2}{a^2} + (1+\nu^D)\log\left(\frac{a}{b}\right)\right\} \tag{26}$$

By using Eq. (25), the flexural stiffness can be determined from the load-displacement curve obtained from the MSP test. In addition, the bending strength can be determined in the same way by using Eq. (26). If the piezoelectric effect is ignored, the solutions reduce the maximum deflections and stress for the elastic plates [38].

4. Results and discussion

4.1. Evaluation of the mechanical and physical properties

MSP tests are practical for understanding the fracture behavior of brittle materials using small test specimens [39]. A load-deflection curve was obtained from the conducted MSP test, and Young's modulus Y_{11} was obtained from Eq. (25) using the load-deflection curve. From the load-deflection curve, a straight line with a slope reduced by 5 % was drawn from the straight elastic line, and the maximum load between the straight lines was defined as the critical load P_Q. The bending strength σ_f was then obtained through Eq. (26) using this critical load. Fig. 6 gives typical load-deflection curves of the KNN-epoxy and KNN-GFRP samples as shown in common piezoelectric ceramics [39]. As expected, the critical load of the KNN-GFRP sample was larger than that of the KNN-epoxy sample. Fig. 7 shows the bending strengths of the KNN-epoxy and KNN-GFRP samples. Here, the MSP specimens were not polarized, so the induced electric field of the composite specimens due to the applied load was ignored. In this case, $\nu^D = \nu_{12}$ could be used. The Poisson's ratio of the composite material was assumed to be $\nu_{12} = 0.37$,

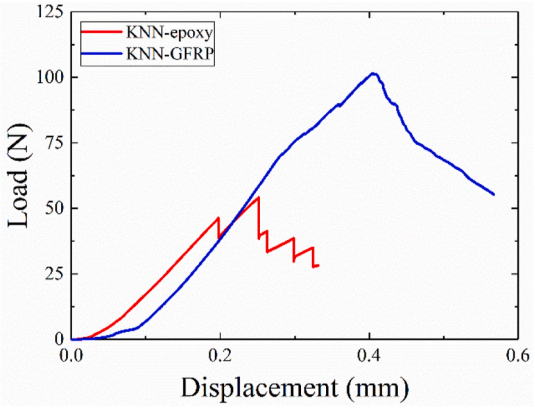

Fig. 6. Load versus displacement curve for the MSP test.

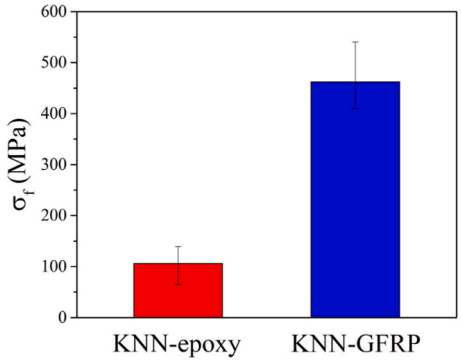

Fig. 7. Bending strengths of the KNN-epoxy and KNN-GFRP samples.

Table 1
Results of the MSP tests and a comparison of the bending properties of piezoelectric materials.

	σ_f (MPa)	E_{MSP} (mJ)	
KNN-epoxy	106	1.70	This work
KNN-GFRP	462	11.8	This work
70 vol%PZT/30 vol%Pt	90		[40]
PZT–15 vol% Ag composite	129		[41]
PZT/ZnO nanowhiskers	120		[42]
PZT/ZnO nanowhiskers/0.5 wt% Nb_2O_5	128		[42]
PZT-5A bracketed by Kapton layers	186.6		[43]
0-3 polymer composite with 0.1 vol%PZT	80		[44]
50%PZT/50%PVDF with 0.3% carbon fiber	31.321		[45]
KNN-CFRP	850		[46]
$BaTiO_3$-CFRP	804		[46]
PZT/carbon black/epoxy composite	65		[47]
PZT (PIC 151)	64.8		[48]
PZT(P-7)		0.28[a]	[39]
PZT	87		[49]
PZT-5A	140.4		[44]
PZT-5H	114.8		[44]
PZT-4	123.2		[44]
PZT-8	127.5		[44]
quenched $(Bi_{0.5}Na_{0.5})TiO_3$ (BNT) ceramics	227		[50]
single-crystal PMN-PT	60.6		[44]
single-crystal PMN-PZT	44.9		[44]

[a] MSP test.

which is the same as the Poisson's ratio of epoxy. The bending strength of the composite material was about 4.4 times that of the resin.

Table 1 lists the bending strength σ_f and MSP energy E_{MSP} for the KNN-GFRP and KNN-epoxy samples. The E_{MSP} was calculated from the area under the load-displacement curve up to the maximum load. The MSP energy of the KNN-GFRP sample was found to be much larger than that of the KNN-epoxy sample. This is due to an increase in the ductility of the composite material because of the presence of glass fibers. Table 1 compares the bending strength and MSP energy of this study with those of piezoelectric composites, piezoelectric ceramics, and single crystals from other studies [39–50]. The bending properties of the KNN-GFRP sample were found to be superior to those of the other piezoelectric materials, except for our previously proposed piezoelectric particle distributed CFRP composite [46].

Fig. 8 shows typical load-displacement curves for the KNN-epoxy and KNN-GFRP samples obtained from the nanoindentation test. It can be seen that the slope of the curve for the KNN-epoxy sample is larger than that for the KNN-GFRP sample. Fig. 9 shows Young's moduli of the KNN-epoxy and KNN-GFRP samples. Since Y_{11} and Y_{33} of the KNN-epoxy sample almost have the same values, the obtained Y_{11} from the MSP test is reasonable considering that epoxy resin is an isotropic elastic material. It was shown that Y_{11} of the composite material is about two times that of the resin and that Y_{33} is about less than half that of the resin. It was also expected that the epoxy resin had not completely penetrated between the glass fibers.

4.2. Evaluation of the piezoelectric properties

Fig. 10 shows the piezoelectric constants d_{33} of the KNN-epoxy and KNN-GFRP samples. The piezoelectric constant of the KNN-GFRP sample was smaller than that of the KNN-epoxy sample, because the GFRP sample has a small volume fraction of piezoelectric nanoparticles due to its glass fiber content. Table 2 presents a comparison of the piezoelectric coefficient d_{33} of the KNN-epoxy and KNN-GFRP samples from this study with the piezoelectric composites from other studies [17,30,31,51–64]. The piezoelectric coefficient d_{31} of some piezoelectric composites [57,60,64,65] is also listed.

4.3. Evaluation of the kinetic energy harvesting performance

Fig. 11 (a) shows the output voltage value for each applied load for the impact energy harvesting test. An output voltage of more than 2 V was obtained due to the compressive stress (0.2 MPa) for both the KNN-epoxy and KNN-GFRP samples. The piezoelectric voltage constants g_{33} of the KNN-epoxy and KNN-GFRP samples were calculated from the slope of Fig. 11, and they were found to be 26.5×10^{-3} V·m/N and 28.9×10^{-3} V·m/N, respectively. From the results of the KNN-epoxy and KNN-GFRP samples, it was interesting to find that the output voltage value of the KNN-GFRP sample with a low volume content and low d_{33} constant was larger than that of the KNN-epoxy sample. One of the reasons for this result is the reduction of the piezoelectric effect due to the breakage of the KNN-epoxy sample, as cracks were observed in the KNN-epoxy sample after the impact test (see Fig. 11 (b)).

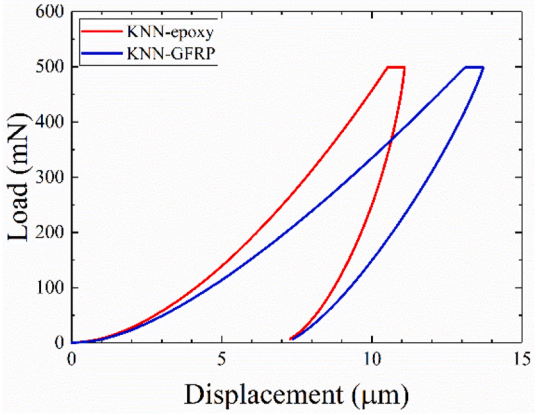

Fig. 8. Load versus displacement curve for the nanoindentation test.

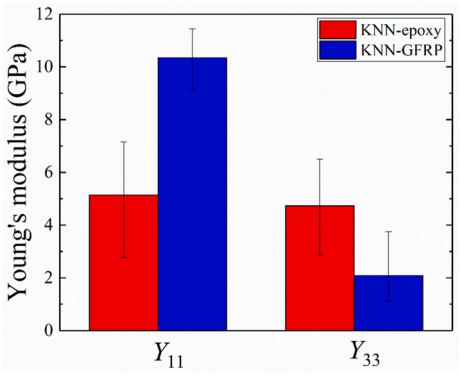

Fig. 9. Young's moduli, Y_{11} and Y_{33}, for the KNN-epoxy and KNN-GFRP samples.

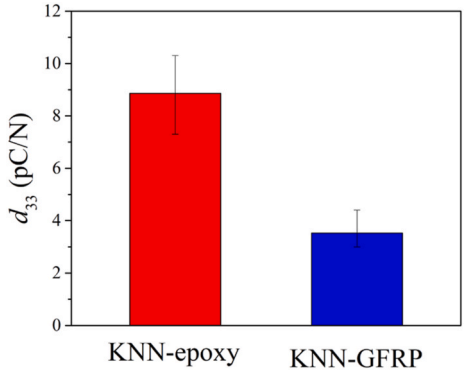

Fig. 10. Piezoelectric coefficients d_{33} for the KNN-epoxy and KNN-GFRP samples.

Fig. 12 (a) shows the output voltage with a time of the KNN-GFRP sample for the damped flexural vibration energy harvesting test. At first, a peak-to-peak of approximately 8 V was obtained. Fig. 12 (b) shows the instantaneous power (black line) and harvested energy (red line) of the KNN-GFRP sample with a load resistance of 10 MΩ. The harvested energy was calculated as

$$U = \frac{1}{R_L}\int V(t)^2 \mathrm{d}t \tag{27}$$

where t is the time. It can be seen that the maximum instantaneous power is approximately 2 μW, and the harvested energy is about 35 nJ. We also performed the damped flexural vibration energy harvesting test on the KNN-epoxy sample. However, when the tip of the KNN-epoxy sample was deflected, it was broken (see Fig. 12 (c)). Hence, the glass fibers work effectively as a reinforcing material for the piezoelectric composite materials. Fig. 13 shows the harvested energy of the KNN-GFRP sample with various values of load resistance. It was confirmed that the maximum harvested energy could be obtained with the appropriate load resistance. However, harvested energy was small. The KNN-GFRP specimen had a large internal resistance. Therefore, a load resistance was larger when the maximized harvested energy was obtained, and harvested energy became small (see Eq. (27)), i.e., it seems that the harvested energy may increase if the internal resistance of the KNN-GFRP specimen reduces. Also, it is well-known that attaching a proof mass to the tip of the cantilever beam and increasing the area of the piezoelectric material improve the harvested energy. In this specimen, similarly, harvested energy can be expected to increase by attaching the proof mass and enlarging the area of the piezoelectric material. Furthermore, since the KNN-GFRP has greater bending strength than ceramic alone, an increase in applied stress can be expected, and a larger increase in harvested energy can also be expected in addition to the effects of the proof mass and area increase.

Table 2
Comparison of the piezoelectric coefficients of piezoelectric composite materials.

Particle	Matrix	Content	d_{33} (pC/N)	d_{31} (pC/N)	
PZT	Epoxy	75 wt%	28	–	[51]
KNN	Epoxy/GFRP	20 vol%	3.5	–	This work
KNN	Epoxy	32 vol%	8.9	–	This work[a]
KNN	Epoxy/CFRP	30 vol%	5.8	–	[30]
KNN	Epoxy/woven CFRP	30 vol%	4.7	–	[52]
KNN	Mullite fiber/polyamide	20 vol%	3	–	[31]
KNN	PVDF	70 vol%	35	–	[53]
KNN	Epoxy	10 vol%	5	–	[54]
KNLN	Epoxy	10 vol%	19	–	[54]
KNLN	Epoxy	10 vol%	13	–	[55]
KNLN-Z	PVDF	80 wt%	39	–	[56]
BTO	Epoxy	32 vol%	5.5	–	[17]
BTO	Epoxy	0.5 vol%	1.16	3.11	[57]
BTO	P(VDF-TrFE)	60 vol%	7–8	–	[58]
BTO	P(VDF-TrFE)	FGC	−9		[59]
BTO-ZnO	Epoxy	1-10 vol%	0.118	0.154	[60]
ZnO	PVDF	0.5 wt%	−32	–	[61]
ZnO	PVDF	0.02 wt%	−9.1	–	[62]
KBT-BA	PVDF	30 vol%	8	–	[63]
CNF	polyvinyl alcohol	6.25 vol%	–	14.5	[64]
$Co_3[Co(CN)_6]_2$	PVDF	5 wt%	37	33	[65]

KNLN: $(K,Na,Li)NbO_3$.
KNLN-Z: $(K,Na,Li)NbO_3$–ZrO_2.
FGC: functionally graded composite.
KBT-BA: $K_{0.5}Bi_{0.5}TiO_3$– $BiAlO_3$.
CNF: cellulose nanofiber.
[a] Comparative material.

5. Conclusions

To obtain piezoelectric composites with sufficient fracture strength, KNN-GFRP composites were developed. The thin plate theory derived a relationship between the maximum displacement and Young's modulus Y_{11} in addition to a relationship between the fracture load and bending strength, including the piezoelectric effect. The bending strength of KNN-GFRP was found to be 462 MPa, which is about 4 times higher than that of KNN-epoxy. Young's moduli Y_{11} and Y_{33} for the KNN-GFRP were obtained from the MSP and nanoindentation tests, respectively. Y_{11} of the KNN-GFRP sample was about two times larger than that of the KNN-epoxy sample. However, Y_{33} of KNN-GFRP sample was about less than half that of the KNN-epoxy sample. The piezoelectric constant measurement showed that the d_{33} of KNN-GFRP is 3.5 pC/N, which is less than half of that of KNN-epoxy. Also, from the impact energy harvesting test, it was found that the output voltages of both samples were almost the same (2.3 V with an impact of 0.2 MPa). Moreover, from the damped flexural vibration energy harvesting test, peak-to-peak of approximately 8 V, maximum instantaneous power of approximately 2 μW and harvested energy of approximately 35 nJ were obtained for the KNN-GFRP, whereas the KNN-epoxy was broken.

Here the electromechanical properties and energy harvesting performance were evaluated for the uncracked material. We believe that the combination of the used test methods can be used to evaluate the electromechanical properties of small piezoelectric materials. On the other hand, how to evaluate the electromechanical properties (including fracture toughness) and energy harvesting performance for the cracked or delaminated material using small test specimens is another theme. This is a challenging theme and our research group is currently working on applying the cracked material.

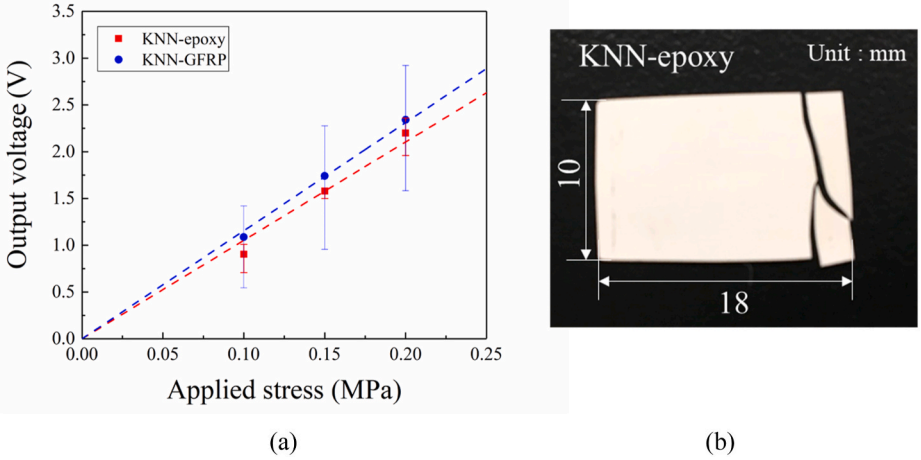

Fig. 11. Results of impact energy harvesting test on the KNN-epoxy and KNN-GFRP samples: (a) Output voltage versus applied compressive stress for the KNN-epoxy and KNN-GFRP samples. (b) a broken KNN-epoxy sample after the test.

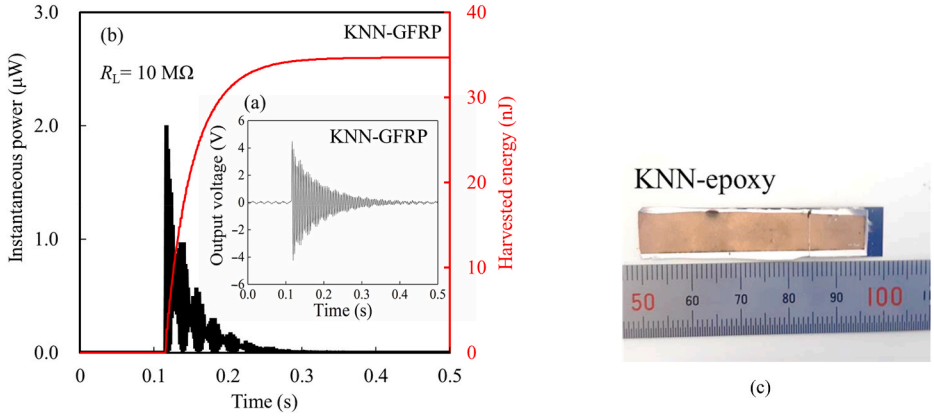

Fig. 12. Results of damped flexural vibration energy harvesting test on the KNN-epoxy and KNN-GFRP samples: (a) measured voltage for the KNN-GFRP sample, (b) instantaneous power and harvested energy for the KNN-GFRP sample, (c) a broken KNN-epoxy sample during the test.

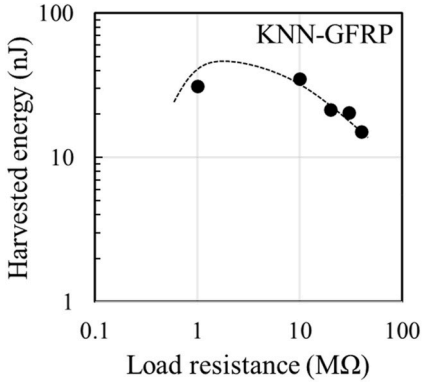

Fig. 13. Harvested energy versus load resistance for the KNN-GFRP sample.

Author statement

Kohei Maruyama: Software, Formal analysis, Investigation, Data Curation, Writing - Original Draft, Visualization.

Yoshihiro Kawakami: Formal analysis, Investigation, Data Curation.

Kotaro Mori: Formal analysis, Investigation, Writing - Review & Editing.

Hiroki Kurita: Validation, Resources, Visualization.

Yu Shi: Writing - Review & Editing.

Yu Jia: Writing - Review & Editing.

Fumio Narita: Conceptualization, Methodology, Writing - Review & Editing, Supervision, Project administration, Funding acquisition.

Declaration of competing interest

The authors declare that they have no known competing financial interests or personal relationships that could have appeared to influence the work reported in this paper.

Acknowledgements

The authors greatly acknowledge the support of this work by Japan Society for the Promotion of Science (JSPS), Core-to-Core Program, grant number: JPJSCCA20200005, and Grant-in-Aid for Scientific Research (A), grant number: 19H00733. We also would like to thank Nippon Chemical Industrial Co. Ltd. for providing KNN particles.

Appendix A

The constitutive relations for the piezoelectric composite materials poled in the x_3- direction are

$$\begin{Bmatrix} \varepsilon_{11} \\ \varepsilon_{22} \\ \varepsilon_{33} \\ 2\varepsilon_{23} \\ 2\varepsilon_{31} \\ 2\varepsilon_{12} \end{Bmatrix} = \begin{bmatrix} s_{11} & s_{12} & s_{13} & 0 & 0 & 0 \\ s_{12} & s_{22} & s_{23} & 0 & 0 & 0 \\ s_{13} & s_{23} & s_{33} & 0 & 0 & 0 \\ 0 & 0 & 0 & s_{44} & 0 & 0 \\ 0 & 0 & 0 & 0 & s_{55} & 0 \\ 0 & 0 & 0 & 0 & 0 & s_{66} \end{bmatrix} \begin{Bmatrix} \sigma_{11} \\ \sigma_{22} \\ \sigma_{33} \\ \sigma_{23} \\ \sigma_{31} \\ \sigma_{12} \end{Bmatrix} + \begin{bmatrix} 0 & 0 & d_{31} \\ 0 & 0 & d_{32} \\ 0 & 0 & d_{33} \\ 0 & d_{24} & 0 \\ d_{15} & 0 & 0 \\ 0 & 0 & 0 \end{bmatrix} \begin{Bmatrix} E_1 \\ E_2 \\ E_3 \end{Bmatrix} \tag{A1}$$

$$\begin{Bmatrix} D_1 \\ D_2 \\ D_3 \end{Bmatrix} = \begin{bmatrix} 0 & 0 & 0 & 0 & d_{15} & 0 \\ 0 & 0 & 0 & d_{24} & 0 & 0 \\ d_{31} & d_{32} & d_{33} & 0 & 0 & 0 \end{bmatrix} \begin{Bmatrix} \sigma_{11} \\ \sigma_{22} \\ \sigma_{33} \\ \sigma_{23} \\ \sigma_{31} \\ \sigma_{12} \end{Bmatrix} + \begin{bmatrix} \epsilon_{11} & 0 & 0 \\ 0 & \epsilon_{22} & 0 \\ 0 & 0 & \epsilon_{33} \end{bmatrix} \begin{Bmatrix} E_1 \\ E_2 \\ E_3 \end{Bmatrix} \tag{A2}$$

where ε_{11}, ε_{22}, ε_{33}, ε_{23}, ε_{31}, and ε_{12} are the components of the strain tensor; σ_{11}, σ_{22}, σ_{33}, σ_{23}, σ_{31}, and σ_{12} are the components of the stress tensor; D_1, D_2, and D_3 are the components of the electric displacement vector; E_1, E_2, and E_3 are the components of the electric field intensity vector; s_{11}, s_{12}, s_{13}, s_{22}, s_{23}, s_{33},s_{44},s_{55}, and s_{66} are the elastic compliances at a constant electric field; d_{31}, d_{32}, d_{33}, d_{24}, and d_{15} are the piezoelectric coefficients; ϵ_{11}, ϵ_{22}, and ϵ_{33} are the permittivities at a constant stress, respectively. The elastic compliances are

$$s_{11} = \frac{1}{Y_{11}},\ s_{12} = -\frac{\nu_{12}}{Y_{11}},\ s_{13} = -\frac{\nu_{13}}{Y_{11}},\ s_{22} = \frac{1}{Y_{22}},\ s_{23} = -\frac{\nu_{23}}{Y_{22}},\ s_{33} = \frac{1}{Y_{33}},\ s_{44} = \frac{1}{G_{23}},\ s_{55} = \frac{1}{G_{13}},\ s_{66} = 2(s_{11} - s_{12}) = \frac{1}{G_{12}} \tag{A3}$$

where Y_{11}, Y_{22}, and Y_{33} are Young's moduli; ν_{12}, ν_{23}, and ν_{31} are Poisson's ratios; G_{12}, G_{23}, and G_{31} are the shear moduli. By assuming that the x_1(fill) and x_2(warp) directions have the same properties, we have the following equations:

$$s_{11} = s_{22},\ s_{13} = s_{23},\ d_{31} = d_{32},\ d_{24} = d_{15},\ \epsilon_{11} = \epsilon_{22} \tag{A4}$$

For a thin plate in the x_1x_2 plane, all the strain and stress components that are related to the x_3 coordinate can be neglected. The constitutive relation becomes

$$\begin{Bmatrix} \varepsilon_{11} \\ \varepsilon_{22} \\ 2\varepsilon_{12} \end{Bmatrix} = \begin{bmatrix} s_{11} & s_{12} & 0 \\ s_{12} & s_{21} & 0 \\ 0 & 0 & s_{66} \end{bmatrix} \begin{Bmatrix} \sigma_{11} \\ \sigma_{22} \\ \sigma_{12} \end{Bmatrix} + \begin{bmatrix} 0 & 0 & d_{31} \\ 0 & 0 & d_{31} \\ 0 & 0 & 0 \end{bmatrix} \begin{Bmatrix} E_1 \\ E_2 \\ E_3 \end{Bmatrix} \tag{A5}$$

$$D_3 = d_{31}(\sigma_{11} + \sigma_{22}) + \epsilon_{33}E_3 \tag{A6}$$

Now, consider the case where the piezoelectric plate is deformed under the open circuit condition, i.e., $D_3 = 0$. From Eq. (A6), the electric field is given by

$$E_3 = -\frac{d_{31}}{\epsilon_{33}}(\sigma_{11} + \sigma_{22}) \tag{A7}$$

By substituting Eq. (A3) and (A6) into Eq. (A5), we obtain

$$\begin{Bmatrix} \varepsilon_{11} \\ \varepsilon_{22} \end{Bmatrix} = \begin{bmatrix} s_{11}^D & s_{12}^D \\ s_{12}^D & s_{11}^D \end{bmatrix} \begin{Bmatrix} \sigma_{11} \\ \sigma_{22} \end{Bmatrix} \tag{A8}$$

where

$$s_{11}^D = \frac{1}{Y_{11}} - \frac{d_{31}^2}{\epsilon_{33}},\ s_{12}^D = -\frac{\nu_{12}}{Y_{11}} - \frac{d_{31}^2}{\epsilon_{33}} \tag{A9}$$

Appendix B

The stress equilibrium equations are as follows:

$$\frac{\partial \sigma_{xx}}{\partial x} + \frac{\partial \sigma_{yx}}{\partial y} + \frac{\partial \sigma_{zx}}{\partial z} = 0$$

$$\frac{\partial \sigma_{xy}}{\partial x}+\frac{\partial \sigma_{yy}}{\partial y}+\frac{\partial \sigma_{zy}}{\partial z}=0 \tag{B1}$$

$$\frac{\partial \sigma_{xz}}{\partial x}+\frac{\partial \sigma_{yz}}{\partial y}+\frac{\partial \sigma_{zz}}{\partial z}=0$$

The stress boundary conditions on the plate surfaces are as follows:

$$\sigma_{zx}=\sigma_{zy}=0\ (z=\pm h/2) \tag{B2}$$

The resultant moments per unit length of the cross-section of the plate are defined as follows:

$$\begin{Bmatrix} M_{xx} \\ M_{yy} \\ M_{xy} \end{Bmatrix}=\int_{-h/2}^{h/2}\begin{Bmatrix} \sigma_{xx} \\ \sigma_{yy} \\ \sigma_{xy} \end{Bmatrix} z\mathrm{d}z \tag{B3}$$

The vertical shear forces per unit length are as follows:

$$\begin{Bmatrix} Q_x \\ Q_y \end{Bmatrix}=\int_{-h/2}^{h/2}\begin{Bmatrix} \sigma_{zx} \\ \sigma_{zy} \end{Bmatrix} \mathrm{d}z \tag{B4}$$

If we multiply the first and second terms of Eq. (B1) by $z\mathrm{d}z$ and integrate from $-h/2$ to $h/2$ while taking into account the boundary conditions (B2) and neglecting the h^3 terms, we shall obtain the results.

$$\frac{\partial M_{xx}}{\partial x}+\frac{\partial M_{yx}}{\partial y}-Q_x=0$$

$$\frac{\partial M_{xy}}{\partial x}+\frac{\partial M_{yy}}{\partial y}-Q_y=0 \tag{B5}$$

If the third Eq. (B1) is multiplied by $\mathrm{d}z$ and integrated from $-h/2$ to $h/2$ while neglecting the h^3 terms, we obtain

$$\frac{\partial Q_x}{\partial x}+\frac{\partial Q_y}{\partial y}+q=0 \tag{B6}$$

where q is a uniform load applied to this plate. By eliminating Q_x and Q_y from Eq. (B5) and Eq. (B6), we have

$$\frac{\partial^2 M_{xx}}{\partial x^2}+2\frac{\partial^2 M_{xy}}{\partial x \partial y}+\frac{\partial M_{yy}}{\partial y^2}+q=0 \tag{B7}$$

References

[1] F. Narita, Z. Wang, H. Kurita, Z. Li, Y. Shi, Y. Jia, C. Soutis, A review of piezoelectric and magnetostrictive biosensor materials for detection of Covid-19 and other viruses, Adv. Mater. 33 (2021), 2005448, https://doi.org/10.1002/adma.202005448.

[2] M. Katta, R. Sandanalakshmi, Simultaneous tropical disease identification with PZT-5H piezoelectric material including molecular mass biosensor microcantilever collection, Sens. Bio Sens. Res. 32 (2021), 100413, https://doi.org/10.1016/j.sbsr.2021.100413.

[3] Y. Wang, Y. Shi, F. Narita, Design and finite element simulation of metal-core piezoelectric fiber/epoxy matrix composites for virus detection, Sens. Actuators A Phys. 327 (2021) 112742, https://doi.org/10.1016/j.sna.2021.112742.

[4] S. Priya, D.I. Inman, Energy Harvesting Technologies, Springer, 2009.

[5] C.R. Bowen, V.Y. Topolov, H.A. Kim, Modern Piezoelectric Energy-Harvesting Materials, Springer, 2016.

[6] F. Narita, M. Fox, A review on piezoelectric, magnetostrictive, and magnetoelectric materials and device technologies for energy harvesting applications, Adv. Eng. Mater. 20 (2018), 1700743, https://doi.org/10.1002/adem.201700743.

[7] S. Mishra, L. Unnikrishnan, S. Nayak, K.S. Mohanty, Advances in piezoelectric polymer composites for energy harvesting applications: a systematic review, Macromol. Mater. Eng. 303 (2019), 1800463, https://doi.org/10.1002/mame.201800463.

[8] Y. Jia, Review of nonlinear vibration energy harvesting: duffing, bistability, parametric, stochastic and others, J. Intell. Mater. Syst. Struct. 31 (2020) 921–944, https://doi.org/10.1177/1045389X20905989.

[9] Y. Hara, Y. Yamamoto, K. Makihara, Self-sensing state estimation of switch-controlled energy harvesters, J. Intell. Mater. Syst. Struct. 31 (2020) 2326–2341, https://doi.org/10.1177/1045389X20943944.

[10] Y. Hara, K. Otsuka, K. Makihara, Adaptive and robust operation with active fuzzy harvester under nonstationary and random disturbance conditions, Sensors 21 (2021) 3913, https://doi.org/10.3390/s21113913.

[11] C.F. Gao, W.X. Fan, Exact solutions for the plane problem in piezoelectric materials with an elliptic or a crack, Int. J. Solid Struct. 36 (1999) 2527–2540, https://doi.org/10.1016/S0020-7683(98)00120-6.

[12] T.Y. Zhang, C.F. Gao, Fracture behaviors of piezoelectric materials, Theor. Appl. Fract. Mech. 41 (2004) 339–379, https://doi.org/10.1016/j.tafmec.2003.11.019.

[13] Y. Shindo, F. Narita, M. Mikami, Double torsion testing and finite element analysis for determining the electric fracture properties of piezoelectric ceramics, J. Appl. Phys. 97 (2005), 114109, https://doi.org/10.1063/1.1925331.

[14] F. Narita, Y. Shindo, F. Saito, Cyclic fatigue crack growth in three-point bending PZT ceramics under electromechanical loading, J. Am. Ceram. Soc. 90 (2007) 2517–2524, https://doi.org/10.1111/j.1551-2916.2007.01774.x.

[15] L. Qi, Y. Shi, L. Liu, C. Gao, Effect of Maxwell stress on a moving crack with polarization saturation region in ferroelectric solid, Meccanica 53 (2018) 3037–3045, https://doi.org/10.1007/s11012-018-0856-9.

[16] M. Xie, Y. Zhang, M.J. Kraśny, C. Bowen, H. Khanbareh, N. Gathercole, Flexible and active self-powered pressure, shear sensors based on freeze casting ceramic-polymer composites, Energy Environ. Sci. 11 (2018) 2919–2927, https://doi.org/10.1039/C8EE01551A.

[17] Z. Wang, F. Narita, Corona poling conditions for barium titanate/epoxy composites and their unsteady wind energy harvesting potential, Adv. Eng. Mater. 21 (2019), 1900169, https://doi.org/10.1002/adem.201900169.

[18] Z. Wang, F. Narita, Fabrication of potassium sodium niobate nano-particle/polymer composites with piezoelectric stability and their application to unsteady wind energy harvesters, J. Appl. Phys. 126 (2019), 224501, https://doi.org/10.1063/1.5127937.

[19] G. D'Ambrogio, O. Zahhaf, Y. Hebrard, M.Q. Le, P.J. Cottinet, J.F. Capsal, Micro-structuration of piezoelectric composites using dielectrophoresis: toward

application in condition monitoring of bearings, Adv. Eng. Mater. 23 (2021), 2000773, https://doi.org/10.1002/adem.202000773.
[20] S.K. Panda, J. Srinivas, Electro-structural analysis and optimization studies of laminated composite beam energy harvester, Mech. Adv. Mater. Struct. in press, Doi:10.1080/15376494.2021.1922787.
[21] A. Alsaadi, Y. Shi, L. Pan, J. Tao, Y. Jia, Vibration energy harvesting of multifunctional carbon fibre composite laminate structures, Compos. Sci. Technol. 178 (2019) 1–10, https://doi.org/10.1016/j.compscitech.2019.04.020.
[22] Y. Jia, X. Wei, L. Xu, C. Wang, P. Lian, S. Xue, A. Al-Saadi, Y. Shi, Multiphysics vibration FE model of piezoelectric macro fibre composite on carbon fibre composite structures, Compo. B 161 (2019) 376–385, https://doi.org/10.1016/j.compositesb.2018.12.081.
[23] Y. Liu, S. Du, C. Micallef, Y. Jia, Y. Shi, D.J. Hughes, Optimisation and management of energy generated by a multifunctional MFC-integrated composite chassis for rail vehicles, Energies 13 (2020) 2720, https://doi.org/10.3390/en13112720.
[24] S.S. Ham, G.-J. Lee, D.Y. Hyeon, Y.-g. Kim, Y.-w. Lim, M.K. Lee, J.J. Park, G. T. Hwang, S. Yi, C.K. Jeong, K.I. Park, Kinetic motion sensors based on flexible and lead-free hybrid piezoelectric composite energy harvesters with nanowires-embedded electrodes for detecting articular movements, Composites Part B 212 (2019), 108705, https://doi.org/10.1016/j.compositesb.2021.108705.
[25] J. Xing, H. Chen, L. Jiang, C. Zhao, Z. Tan, Y. Huang, B. Wu, Q. Chen, D. Xiao, J. Zhu, High performance $BiFe_{0.9}Co_{0.1}O_3$ doped KNN-based lead-free ceramics for acoustic energy harvesting, Nano Energy 84 (2021), 105900, https://doi.org/10.1016/j.nanoen.2021.105900.
[26] N. Sezer, M.A. Koç, A comprehensive review on the state-of-the-art of piezoelectric energy harvesting, Nano Energy 80 (2021), 105567, https://doi.org/10.1016/j.nanoen.2020.105567.
[27] F. Cakmak Bolat, S. Basaran, M. Kara, Investigation of energy harvesting in composite beams with different lamination angles under dynamic effects, Compos. Struct. 270 (2021), 114056, https://doi.org/10.1016/j.compstruct.2021.114056.
[28] M.Y. Hwang, L.H. Lang, Characteristics and fabrication of piezoelectric GFRP using smart resin prepreg for detecting impact signals, Compos. Sci. Technol. 167 (2018) 224–233, https://doi.org/10.1016/j.compscitech.2018.08.002.
[29] F. Narita, H. Nagaoka, Z. Wang, Fabrication and impact output voltage characteristics of carbon fiber reinforced polymer composites with lead-free piezoelectric nano-particles, Mater. Lett. 236 (2019) 487–490, https://doi.org/10.1016/j.matlet.2018.10.174.
[30] Z. Wang, H. Kurita, H. Nagaoka, F. Narita, Potassium sodium niobate lead-free piezoelectric nanocomposite generators based on carbon-fiber-reinforced polymer electrodes for energy-harvesting structures, Compos. Sci. Technol. 199 (2020), 108331, https://doi.org/10.1016/j.compscitech.2020.108331.
[31] K. Takaishi, Y. Kubota, H. Kurita, Z. Wang, F. Narita, Fabrication and electromechanical characterization of mullite ceramic fiber/thermoplastic polymer piezoelectric composites, J. Am. Ceram. Soc. 105 (2022) 308–316, https://doi.org/10.1111/jace.18047.
[32] ISO 14577-1:2015 Metallic materials, Instrumented Indentation Test for Hardness and Materials Parameters — Part, vol. 1, Test method, 2015.
[33] Y. Kawakami, Increasing vibration power generation energy by increasing the area of $BaTiO_3$ thick film formed on stainless-steel substrate by aerosol deposition, J. Ceram. Soc. Jpn. 129 (2021) 217–222, https://doi.org/10.2109/jcersj2.20146.
[34] H.F. Tiersten, Linear Piezoelectric Plate Vibration, Plenum Press, New York, 1969, https://doi.org/10.1007/978-1-4899-6453-3.
[35] G. Beckers, B. Dehez, Modelling of electric field and stress in piezoelectric composite plates under bending load, in: 2014 Joint IEEE International Symposium on the Applications of Ferroelectric, International Workshop on Acoustic Transduction Materials and Devices & Workshop on Piezoresponse Force Microscopy, 2014, pp. 1–4, https://doi.org/10.1109/ISAF.2014.6922962.
[36] A.E.H. Love, The small free vibrations and deformation of a thin elastic shell, Phil. Trans. Roy. Soc. Lond. 179 (1888) 491–546.
[37] L.D. Landau, E.M. Lifshitz, Theory of Elasticity, third ed., vol. 7, Butterworth-Heinemann, 1986.
[38] J.-F. Li, R. Watanabe, Fracture toughness of Al_2O_3-particle-dispersed Y_2O_3-partially stabilized zirconia, J. Am. Ceram. Soc. 78 (1995) 1079–1082, https://doi.org/10.1111/j.1151-2916.1995.tb08441.x.
[39] Y. Shindo, F. Narita, K. Horiguchi, Y. Magara, M. Yoshida, Electric fracture and polarization switching properties of piezoelectric ceramic PZT studied by the modified small punch test, Acta Mater 51 (2003) 4773–4782, https://doi.org/10.1016/S1359-6454(03)00303-3.
[40] K. Takagi, J.F. Li, S. Yokoyama, R. Watanabe, Fabrication and evaluation of PZT/Pt piezoelectric composites and functionally graded actuators, J. Eur. Ceram. Soc. 23 (2003) 1577–1583, https://doi.org/10.1016/S0955-2219(02)00407-7.
[41] H.L. Zhang, J.F. Li, B.P. Zhang, W. Jiang, Enhanced mechanical properties in Ag-particle-dispersed PZT piezoelectric composites for actuator applications, Mater. Sci. Eng., A 498 (2008) 272–277, https://doi.org/10.1016/j.msea.2008.07.073.
[42] D.W. Wang, M.S. Cao, J. Yuan, Q.L. Zhao, H.B. Li, D.Q. Zhang, S. Agathopoulos, Enhanced piezoelectric and ferroelectric properties of Nb_2O_5 modified lead zirconate titanate-based composites, J. Am. Ceram. Soc. 94 (2011) 647–650, https://doi.org/10.1111/j.1551-2916.2010.04309.x.
[43] S.R. Anton, A. Erturk, D.J. Inman, Bending strength of piezoelectric ceramics and single crystals for multifunctional load-bearing applications, IEEE Trans. Ultrason. Ferroelectrics Freq. Control 59 (2012) 1085–1092, https://doi.org/10.1109/TUFFC.2012.2299.
[44] N.K. James, D. Van Den Ende, U. Lafont, S. Van Der Zwaag, W.A. Groen, Piezoelectric and mechanical properties of structured PZT-epoxy composites, J. Mater. Res. 28 (2013) 635–641, https://doi.org/10.1557/jmr.2012.428.
[45] H. Yang, J. Pei, S. Cui, Q. Guo, R. Li, Performance analysis of fiber reinforced piezoelectric lead zirconate titanate/poly(Vinylidene fluoride) composites, Materials Express 8 (2018) 511–520, https://doi.org/10.1166/mex.2018.1459.
[46] H. Kurita, Z. Wang, H. Nagaoka, F. Narita, Fabrication and mechanical properties of carbon-fiber-reinforced polymer composites with lead-free piezoelectric nanoparticles, Sensor. Mater. 32 (2020) 2453–2462, https://doi.org/10.18494/SAM.2020.2820.
[47] Z. Tang, H. Hao, B. Wan, M. Cao, Z. Yao, H. Liu, Preparation and properties of epoxy piezoelectric vibration reduction composites, J. Wuhan Univ. Technol.-Materials Sci. Ed. 36 (2021) 44–49, https://doi.org/10.1007/s11595-021-2376-z.
[48] T. Fett, D. Munz, G. Thun, Tensile and bending strength of piezoelectric ceramics, J. Mater. Sci. Lett. 18 (1999) 1899–1902, https://doi.org/10.1023/A:1006698724548.
[49] H. Zhang, S. Yang, S. Yang, D. Kong, B.P. Zhang, Y. Zhang, Reliability enhancement in nickel-particle-dispersed alkaline niobate piezoelectric composites and actuators, J. Eur. Ceram. Soc. 31 (2011) 795–800, https://doi.org/10.1016/j.jeurceramsoc.2010.11.025.
[50] Y. Takagi, H. Nagata, T. Takenaka, Effects of quenching on bending strength and piezoelectric properties of $(Bi_{0.5}Na_{0.5})TiO_3$ ceramics, J. Asian Ceram. Soc. 8 (2020) 277–283, https://doi.org/10.1080/21870764.2020.1732020.
[51] S. Eßlinger, S. Geller, K. Hohlfeld, S. Gebhardt, A. Michaelis, M. Gude, A. Schönecker, P. Neumeister, Novel poling method for piezoelectric 0-3 composites and transfer to series production, Sensor. Actuator. 270 (2018) 231–239, https://doi.org/10.1016/j.sna.2017.12.062.
[52] Y. Yu, F. Narita, Evaluation of electromechanical properties and conversion efficiency of piezoelectric nanocomposites with carbon-fiber-reinforced polymer electrodes for stress sensing and energy harvesting, Polymers 13 (2021) 3184, https://doi.org/10.3390/polym13183184.
[53] B. Ponraj, R. Bhimireddi, K.B.R. Varma, Effect of nano- and micron-sized $K_{0.5}Na_{0.5}NbO_3$ fillers on the dielectric and piezoelectric properties of PVDF composites, J.Adv. Ceram. 5 (2016) 308–320, https://doi.org/10.1007/s40145-016-0204-2.
[54] D.B. Deutz, N.T. Mascarenhas, S. van der Zwaag, W.A. Groen, Enhancing energy harvesting potential of $(K,Na,Li)NbO_3$-epoxy composites via Li substitution, J. Am. Ceram. Soc. 100 (2017) 1108–1117, https://doi.org/10.1111/jace.14698.
[55] N.K. James, D.B. Deutz, R.K. Bose, S. van der Zwaag, P. Groen, High piezoelectric voltage coefficient in structured lead-free (K, Na, Li)NbO_3 particulate-epoxy composites, J. Am. Ceram. Soc. 99 (2016) 3957–3963, https://doi.org/10.1111/jace.14428.
[56] K. Yu, S. Hu, W. Yu, J. Tan, Piezoelectric and dielectric properties of $((K_{0.475}Na_{0.495}Li_{0.03})NbO_3$-$0.003ZrO_2)$/PVDF composites, J. Electron. Mater. 48 (2019) 2329–2337, https://doi.org/10.1007/s11664-019-06978-1.
[57] U. Sundar, Z. Lao, K. Cook-Chennault, Investigation of piezoelectricity and resistivity of surface modified barium titanate nanocomposites, Polymers 11 (2019) 2123, https://doi.org/10.3390/polym11122123.
[58] C. Carbone, M. Benwadih, G. D'Ambrogio, M.Q. Le, J.F. Capsal, P.J. Cottinet, Influence of matrix and surfactant on piezoelectric and dielectric properties of screen-printed $BaTiO_3$/PVDF composites, Polymers 13 (2021) 2166, https://doi.org/10.3390/polym13132166.
[59] Z. Wang, K. Maruyama, F. Narita, A novel manufacturing method and structural design of functionally graded piezoelectric composites for energy-harvesting, Mater. Des. 214 (2022), 110371, https://doi.org/10.1016/j.matdes.2021.110371.
[60] W. Tuff, P. Manghera, J. Tilghman, E. van Fossen, S. Chowdhury, S. Ahmed, S. Banerjee, $BaTiO_3$-epoxy-ZnO-based multifunctional composites: variation in electron transport properties due to the interaction of ZnO nanoparticles with the composite microstructure, J. Electron. Mater. 48 (2019) 4987–4996, https://doi.org/10.1007/s11664-019-07292-6.
[61] B. Mahanty, S.K. Ghosh, S. Jana, Z. Mallick, S. Sarkara, D. Mandal, ZnO nanoparticle confined stress amplified all-fiber piezoelectric nanogenerator for self-powered healthcare monitoring, Sustain. Energy Fuels 5 (2021) 4389–4400, https://doi.org/10.1039/D1SE00444A.
[62] C. Chen, R. Zhang, J. Zhu, X. Qian, J. Zhu, X. Ye, M. Zhang, Direct writing polyvinylidene difluoride thin films by intercalation of nano-ZnO, Polym. Eng. Sci. 61 (2021) 1802–1809, https://doi.org/10.1002/pen.25701.
[63] S. Dwivedi, M. Badole, T. Pareek, S. Kumar, Multifunctional lead-free $K_{0.5}Bi_{0.5}TiO_3$-based ceramic reinforced PVDF matrix composites, J. Alloys Compd. 871 (2021), 159616, https://doi.org/10.1016/j.jallcom.2021.159616.
[64] E.S. Choi, H.C. Kim, R.M. Muthoka, P.S. Panicker, D.O. Agumba, J. Kim, Aligned cellulose nanofiber composite made with electrospinning of cellulose nanofiber - polyvinyl alcohol and its vibration energy harvesting, Compos. Sci. Technol. 209 (2021), 108795, https://doi.org/10.1016/j.compscitech.2021.108795.
[65] L. Yang, T. Qiu, M. Shen, H. He, H. Huang, Metal-organic frameworks $Co_3[Co(CN)_6]_2$: a promising candidate for dramatically reinforcing the piezoelectric activity of PVDF, Compos. Sci. Technol. 196 (2020), 108232, https://doi.org/10.1016/j.compscitech.2020.108232.